energies

MDPI

Article

Numerical and Parametric Study on Open-Type Ceiling Radiant Cooling Panel with Curved and Segmented Structure

Minzhi Ye [1], Ahmed A. Serageldin [2,3,*] and Katsunori Nagano [2,*]

[1] Graduate School of Engineering, Hokkaido University, Sapporo 060-8628, Japan
[2] Division of Human Environmental System, Faculty of Engineering, Hokkaido University, N13-W8, Kita Ku, Sapporo 060-8628, Japan
[3] Department of Mechanical Engineering, Shoubra Faculty of Engineering, Benha University, Cairo 11629, Egypt
* Correspondence: ahmed.serageldin@eng.hokudai.ac.jp (A.A.S.); nagano@eng.hokudai.ac.jp (K.N.); Tel.: +81-080-5747-5714 (A.A.S.)

Abstract: A suspended open-type ceiling radiant cooling panel (CRCP) has been proposed recently. The main challenge is improving its cooling performance to overcome limitations for extensive use. Therefore, this study aims to optimize the design of CRCPs with curved and segmented structure to enhance heat transfer. A three-dimensional CFD model was developed to investigate the cooling capacity and heat transfer coefficient of the CRCPs installed inside a single enclosed room. Panel structure was determined based on four dependent parameters: the panel curvature width (L, m), the panel curvature radius (r, m), the void distance (d, m) between each panel or panel segment, and the panel coverage area (A_c, m^2). The panel surface area (A_s, m^2) and the ratio of panel curvature width to radius (L/r) were also examined. A total of 35 designs were compared under 7 different cooling load conditions, and 245 cases were carried out. The results show that the nominal cooling capacity and heat transfer coefficient rise with increasing curvature radius and decreasing curvature width. The void distance plays the most crucial role in influencing cooling performance. It is possible to simultaneously improve cooling performance, achieve uniform temperature distribution, and reduce the number of panels through structure optimization.

Keywords: ceiling radiant cooling panel; parametric analysis; CFD simulation; cooling capacity

Citation: Ye, M.; Serageldin, A.A.; Nagano, K. Numerical and Parametric Study on Open-Type Ceiling Radiant Cooling Panel with Curved and Segmented Structure. *Energies* **2023**, *16*, 2705. https://doi.org/10.3390/en16062705

Academic Editors: Alessandro Cannavale and Ubaldo Ayr

Received: 14 February 2023
Revised: 28 February 2023
Accepted: 9 March 2023
Published: 14 March 2023

1. Introduction

Radiant ceiling panel systems have been a matter of great concern [1] in recent decades, considering their benefits of high thermal comfort level and energy-saving potential [2]. Such systems can be combined with renewable energy, as they generally use water as the thermal medium for space heating and cooling. Therefore, the use of radiant ceiling panel systems is a popular alternative heating and cooling method to conventional air source systems, and such systems are widely applied as energy efficiency technologies. These systems have been applied in various building types, such as high-volume halls (e.g., vehicle repair shops and markets) [3], office buildings [4,5], schools [6], hospitals [7], and residential buildings [8]. Ceiling radiant cooling panel (CRCP) systems are typically used for cooling, commonly consisting of a metal panel, a water pipe directly or indirectly touching the panel, and insulation on the top of the panel surface [9,10]. The insulation layer above the panel is expected to insulate the heat transfer between the panel and the ceiling to activate heat transfer on the bottom surface towards the conditioned space. However, upward heat loss is inevitable. Thus, some researchers have focused on improving the insulation layer to reduce the heat flux to increase the cooling capacity of the CRCP [11]. On the other hand, an open-type CRCP, also called a suspended radiant ceiling panel (SRCP) [12] or suspended ceiling radiant panel (CRP) [13] has recently come to public attention. Unlike the top-insulated type, an open-type CRCP is installed separately from

the ceiling, excluding insulation between the panel top and ceiling. Due to the characteristic of convenient and flexible installation, this type is also widely used in existing or new buildings in practice [14].

Nevertheless, CRCPs are still associated with risk of dew condensation on the cooling surface, as in other radiant cooling systems. Furthermore, high manufacturing and installation costs also limit their practical applications. Therefore, it is urgently required to address these issues by improving system performance through the use of advanced strategies [15]. In recent studies, combining CRCPs with an air circulating strategy has been proposed as an effective method. Shakya et al. [16] proposed a hybrid system coupling natural ventilation and a desiccant dehumidification system with a CRCP. The cooling capacity and thermal comfort can be significantly enhanced by the proposed hybrid system. The proposed hybrid system can save 77% and 61% primary energy consumption compared to a conventional all-air system and radiant cooling system, respectively. Jeong and Mumma [17] investigated the mixed convection effect on the cooling capacity of a CRCP. The results revealed that the total cooling capacity of a CRCP can be increased by 5–35% by the combination of natural and mechanical ventilation. Shin et al. [18] combined an open-type CRCP with air circulators to enhance cooling capacity and energy performance. The results showed that the cooling capacity was enhanced by 26.4%, and energy consumption was reduced by 26.4% compared with a conventional CRCP system. In summary, increasing the convection in the conditioned space of a CRCP is impactful in improving the cooling performance and reducing the energy consumption of CRCP systems. Another possibility is to reform the structural design of the CRCP to achieve the same effect of convection enhancement [19], which has been investigated in many studies.

Moreover, it is crucial to investigate the effect of each parameter through parametric studies to achieve an optimal overall panel structure and arrangement. Statistical analysis is necessary to optimize and prioritize the design considering the conflict between different desires in terms of cooling capacity, panel surface temperature, temperature distribution, or other factors. For instance, with respect to the design of a thermoelectric radiant panel (TCRP) system, Lim et al. [20] carried out a parametric study consider spacing, panel and insulation thickness, outdoor air temperature, and heat sink. The authors evaluated the effects of design factors and operation conditions on the cooling performance. The results proved that the spacing and outdoor air temperature are the main factors that influence of the cooling performance of the TCRP. Luo et al. [21] conducted a parametric study on the thickness of aluminum panels and insulation. The optimum thickness of aluminum panels and insulation was found to be around 1–2 mm and 40–50 mm, respectively.

In this study, an open-type CRCP with a segmented and curved shape was proposed, which is expected to achieve better cooling performance through the structural optimization of the design. The objectives of this study are to evaluate the effects of the panel design parameters of the novel panel structure and explore the ideal design to maximize the cooling capacity of CRCP in terms of energy and cost reduction and achieving the required thermal comfort level. A parametric analysis was conducted of the proposed novel open-type ceiling radiant cooling panel (CRCP), which has curved shapes and voids between the adjacent panels. A three-dimensional CFD simulation model was developed to study the cooling capacity and heat transfer coefficient of the panel in an enclosed space. Thirty-five panel designs were examined and compared with the reference panels. The influence of four independent and two dependent panel design parameters were investigated based on the calculation of nominal cooling capacity, heat transfer coefficient, airflow, and indoor temperature distribution. Finally, the optimal panel design was discussed and recommended according to both cooling performance and thermal comfort.

2. Design of Ceiling Radiant Ceiling Panels (CRCPs)

2.1. Literature Review of CRCP Design

As stated above, it is important to increase the efficiency and cooling performance of CRCPs system through the use of advanced strategies. Table 1 lists previous studies

that aimed to enhance the cooling capacity of panels by via panel design. The designs of panels included the water tube/water channel configuration design, panel configuration design, panel distribution arrangement design, and panel material design. The results showed that the cooling capacity or even the uniformity of the indoor air temperature field can be substantially improved by applying novel design strategies. Serageldin et al. [22] compared nine different open-type CRCPs including two curved CRCPs with voids by numerical simulation, considering the heat flux, heat transfer coefficient, and indoor operative temperature. The results illustrated that changing the panel shape to a curved design and adding voids can increase the radiation heat transfer coefficient by 31% and convection heat transfer by 174% and decrease the indoor air temperature by 1 K.

Table 1. Studies on CRCP structure design.

Literature	Panel Type	Methodology	Design Strategy	Improvement Results
Mosa et al. [23,24]	SRCP	Numerical simulation	Serpentine and dendritic flow channel design	The dendritic architecture allows for a significant improvement in the cooling panel performance.
Hassan and Kaood [25]	SRCP	CFD simulation	Application of internal longitudinal fins	The presented balanced design enhances the cooling capacity and cooling rate by 1.54 and 17.7%, respectively.
Radzai et al. [26]	RCP	CFD simulations	New RCP serpentine-based flow configuration	The proposed designs have the potential to improve the overall efficiency of RCP in terms of temperature distribution, cooling capacity, and pressure.
Labat et al. [12]	SRCP	Genetic algorithm	Arrangement of multiple panels on the ceiling	The uniformity of the temperature field can be significantly improved by using 10 panels or more compared with using a single panel.
Shin et al. [27]	Open type	Experiments and CFD simulation	Open-type CRCP installed with void areas between adjacent ceiling panels	The open-type CRCP can provide 54–80% higher nominal cooling capacity than a conventional closed-type CRCP.
Radwan et al. [28]	Open type	CFD simulation	New multisegmented mini-channel-based CRCP	The design can accomplish the same cooling capacity and identical indoor air temperature by using a higher panel surface temperature.
Zhang et al. [13]	Open type	Experiments	A new type of CRCP with inclined aluminum fins	The cooling capacity of the CRCP with inclined fins is about 19% higher than that of a suspended panel.
Lv et al. [29]	RCP	Experiments	A novel grooved radiant ceiling panel filled with heat transfer liquid	The cooling capacity of this radiant panel was 18–25% higher than that of traditional metal radiant panels.
Ning et al. [30]	CRCP	CFD simulation	CRCP with a thin air layer	The cooling capacities are increased by 43–46% compared to the original CRCP.
Xing and Li [11]	CRCP	Experiments	Replacement of the radiation shield with a convection shield	The improved inbuilt air gap has a better synergy in improving cooling capacity and anticondensation ability.

2.2. Parameter Design of Curved Open-Type CRCPs

The aim of this study is to explore the inter-relationship between panel design (including curved structure and panel distribution designs) and cooling performance. It was urgently required to determine the optimal design, which can balance contradictory goals in terms of enhancing cooling capacity and maintaining thermal comfort. Therefore, four independent parameters were used to determine the panel shape, as shown in Figure 1: the panel curvature width (L, m), the curvature radius (r, m), the void distance between each panel or panel segment (d, m), and the panel coverage area (A_c, m^2). Two dependent parameters were also investigated: the ratio of panel curvature width to radius (L/r) and panel surface area (A_s, m^2). The L/r ratio is a parameter affecting the curvature shape of the panel. The curvature of the panel increases with an increase in the value of L/r. The

panel surface area (A_s) is a parameter depending on all four independent parameters and calculated according to Equation (1). It closely relates to the manufacturing cost. Therefore, it is preferred to minimize the panel surface area in the design stage.

$$A_s = \frac{2\sin^{-1}\left(\frac{L}{2r}\right)}{180} \cdot \pi r \cdot l \cdot n \quad (1)$$

where l is the panel length (m), and n is the panel number related to the panel curvature width (L), void distance (d), and panel coverage area (A_c).

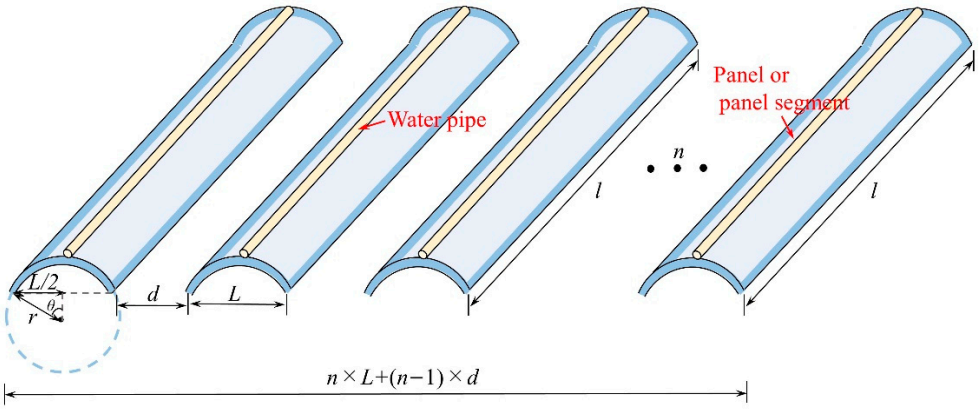

Figure 1. Schematic diagram of the panel and design parameters.

Thirty-five designs were created and compared to show the effect of each parameter. The values of each parameter in each case are summarized in Table 2. The panel curvature width (L) was altered from 0.03 to 0.12 m, the panel curvature radius (r) was altered from 0.03 m to 0.3 m, the void distance (d) was altered from 0 m to 0.33 m, and the panel cover area (A_c) was altered from 7.58 m^2 to 12.96 m^2. Accordingly, the L/r ratio varied from 0 to 2, and the panel surface area (A_s) varied from 2.51 m^2 to 16.90 m^2. When the effect of one independent parameter was examined individually, the other three parameters were held constant. Two dependent parameters—L/r ratio and A_s—were investigated with different panel width and curvature radius values, while the coverage area and void distance were the same. Additionally, four replenished designs were proposed for optimization and verification.

Table 2. Design of parameters.

Design	L (m)	r (m)	d (m)	L/r	A_c (m^2)	A_s (m^2)
1	0.03	0.06	0.03	0.5	12.96	8.18
2	0.06	0.06	0.03	1	12.96	10.28
3	0.09	0.06	0.03	1.5	12.96	11.72
4	0.12	0.06	0.03	2	12.96	16.90
5	0.06	0.03	0.03	2	12.96	14.90
6	0.06	0.09	0.03	0.7	12.96	10.06
7	0.06	0.15	0.03	0.4	12.96	9.96
8	0.06	0.2	0.03	0.3	12.96	9.93
9	0.06	0.3	0.03	0.2	12.96	9.91
10	0.06	0.06	0	1	12.96	13.58
11	0.06	0.06	0.01	1	12.96	13.05
12	0.06	0.06	0.03	1	12.96	10.03
13	0.06	0.06	0.06	1	12.96	7.53
14	0.06	0.06	0.1	1	12.96	5.77
15	0.06	0.06	0.14	1	12.96	4.51
16	0.06	0.06	0.21	1	12.96	3.51
17	0.06	0.06	0.33	1	12.96	2.51

Table 2. *Cont.*

Design	L (m)	r (m)	d (m)	L/r	A_c (m^2)	A_s (m^2)
18	0.06	0.06	0.03	1	11.43	9.05
19	0.06	0.06	0.03	1	10.80	8.53
20	0.06	0.06	0.03	1	10.15	8.02
21	0.06	0.06	0.03	1	8.86	7.02
22	0.06	0.06	0.03	1	7.58	5.77
23	0.1	0.09	0.03	1.1	12.96	11.18
24	0.15	0.2	0.03	0.75	12.96	11.17
25	0.2	0.4	0.03	0.5	12.96	10.85
26	0.3	1	0.03	0.3	12.96	10.80
27	0.16	-	0.03	0	12.96	10.84
28	0.045	0.03	0.03	1.5	12.96	10.09
29	0.135	0.09	0.03	1.5	12.96	12.65
30	0.225	0.15	0.03	1.5	12.96	13.19
31	0.3	0.2	0.03	1.5	12.96	13.73
32	0.03	0.06	0.05	0.5	12.96	6.04
33	0.03	0.06	0.1	0.5	12.96	3.62
34	0.03	0.06	0.05	0.5	11.43	5.38
35	0.03	0.06	0.1	0.5	11.43	3.35

3. Model Development

ANSYS 2020 R2 Fluent commercial software was used to perform computational fluid dynamics (CFD) simulations. A three-dimensional finite-volume model was developed to determine the heat transfer and temperature field. The assumptions applied in this model are listed as follows:

1. The heat transfer is calculated under a steady-state condition;
2. The air density difference is ignored, and only the gravitational force effect is considered;
3. The heat transfer between the water pipe and the panel surface is ignored, and the panel surface temperature is considered uniform;
4. The emissivity is constant and a property of the surface, which is independent of wavelength;
5. The surface is opaque and diffuse, and only the transferred radiation between two surfaces is considered.

3.1. Geometry

The enclosed room is 4 m (Length) × 4 m (Width) × 2.9 m (Height), which has are same dimensions and arrangement as the room model for a suspended flat panel validated by Shin et al. [27]. Twelve cylindrical occupant dummies with dimensions of 0.3 m (D) × 1.1 m (H) are deployed symmetrically in the room to mimic human bodies, generating energy dissipation in the space and representing a cooling load. The panels are suspended 0.3 m beneath the ceiling and arranged along the central line. In the validated case, the panel is one flat, solid panel with dimensions of 3.6 m (Length) × 3.6 m (Width) × 0.03 m (Height), while in other cases with curved and segmented type panels, four independent panel design parameters (L, r, d, and A_c) are set using the design values listed in Table 2. Instead of directly inputting the coverage area (A_c), the number of panels (n) is employed in the geometric drawing, which can be determined according to Equation (2):

$$n = \left\lceil \frac{1}{(L+d)} \cdot \left(\frac{A_c}{l} + d\right) \right\rceil \quad (2)$$

Moreover, the symmetry boundary condition was applied to the middle plane to simplify the modeling and accelerate the simulation speed due to the completely symmetrical characteristic of the room. In this study, all the simulations were conducted in half of the space, as shown in Figure 2.

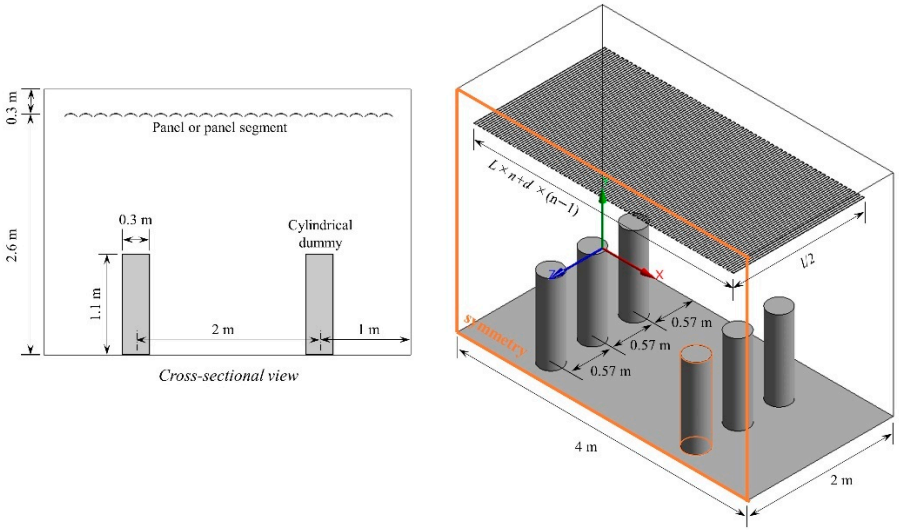

Figure 2. The geometry of the model and a cross-sectional view at the middle plane.

3.2. Mesh

The mesh was generated by the ANSYS Meshing tool using tetrahedron mesh and inflation layers near the cylinder surface (Figure 3a). The grid around the wall, panel, and dummy cylinder surface was refined to address the expected high gradient of temperature by adding an inflation layer with 0.001 m first-layer thickness and a growth rate of 1.2. Mesh-independent analysis was carried out for one curved panel design to minimize the impact of element size on the simulation accuracy. Four different element numbers were selected: 2.2×10^5, 5.9×10^5, 9.3×10^5, 1.4×10^6, 2.1×10^6, 2.6×10^6, and 3.6×10^6. The total heat flux and indoor air temperature varied with an increasing number of elements, as shown in Figure 3b. Therefore, the preferred number of elements was 1,432,275 in the present study, as the results demonstrated a change in heat flux of only 0.17% and a change in average air temperature of only 0.81% compared with the finer mesh.

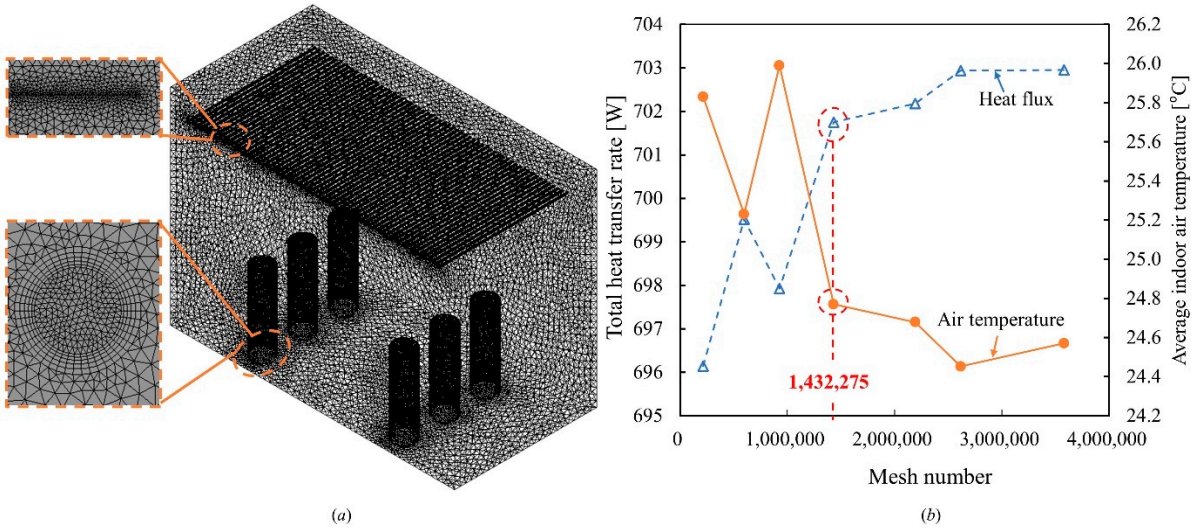

Figure 3. (**a**) Computational mesh used in the present study. (**b**) Mesh-independent analysis results.

3.3. Description of Numerical Equations

3.3.1. Governing Equation

- Mass conservation [31]:

$$\nabla \cdot (\rho \vec{v}) = 0 \tag{3}$$

- Momentum conservation [31]:

$$\nabla \cdot (\rho \vec{v}\vec{v}) = -\nabla p + \nabla \cdot (\bar{\bar{\tau}}) + \rho \vec{g} \tag{4}$$

where the surface stress tensor ($\bar{\bar{\tau}}$, N/m^2) is given by the following equation:

$$\bar{\bar{\tau}} = \mu \left[\left(\nabla \vec{v} + \nabla \vec{v}^{\mathrm{T}} \right) - \frac{2}{3} \nabla \cdot \vec{v} I \right] \tag{5}$$

- Energy conservation [31]:

$$\nabla \cdot (\rho C_{\mathrm{p}} \vec{v} T_{\mathrm{f}}) = \nabla \cdot (k_{\mathrm{f}} \nabla T_{\mathrm{f}}) \tag{6}$$

where ρ is the fluid density (kg/m^3), $\vec{v}$ is the velocity vector (m/s), p is the static pressure (N/m^2), $\rho \vec{g}$ is the gravitational body force (N/m^3), μ is the molecular viscosity (kg/m·s), I is the unit tensor, C_{p} is the specific heat capacity (J/kg·K), T_{f} is the fluid temperature (K), and k_{f} is the fluid thermal conductivity (W/m·k).

3.3.2. Turbulent Model

The standard k-ε model proposed by Launder and Spalding (1972) is used to describe the effect of turbulence. The equations for turbulent kinetic energy k (m^2/s^2) and the turbulent dissipation rate ε (m^2/s^3) are expressed as Equations (7) and (8) [31], respectively:

- Turbulent kinetic energy:

$$\frac{\partial}{\partial \mathrm{t}}(\rho k) + \frac{\partial}{\partial x_{\mathrm{i}}}(\rho k u_{\mathrm{I}}) = \frac{\partial}{\partial x_{\mathrm{j}}} \left[\left(\mu + \frac{\mu_{\mathrm{t}}}{\sigma_{\mathrm{k}}} \right) \frac{\partial k}{\partial x_{\mathrm{j}}} \right] + G_{\mathrm{k}} + G_{\mathrm{b}} - \rho \varepsilon - Y_{\mathrm{M}} + S_{\mathrm{k}} \tag{7}$$

- Turbulent dissipation rate:

$$\frac{\partial}{\partial \mathrm{t}}(\rho \varepsilon) + \frac{\partial}{\partial \mathrm{x_i}}(\rho \varepsilon I) = \frac{\partial}{\partial x_{\mathrm{j}}} \left[\left(\mu + \frac{\mu_{\mathrm{t}}}{\sigma_{\varepsilon}} \right) \frac{\partial \varepsilon}{\partial x_{\mathrm{j}}} \right] + C_{1\varepsilon} \frac{\varepsilon}{k} (G_{\mathrm{k}} + C_{3\varepsilon} G_{\mathrm{b}}) - C_{2\varepsilon} \rho \frac{\varepsilon^2}{k} + S_{\varepsilon} \tag{8}$$

where μ_{t} is the turbulent viscosity (kg/m·s), as follows.

$$\mu_{\mathrm{t}} = \rho C_{\mu} \frac{k^2}{\varepsilon} \tag{9}$$

where u_{i} is the velocity, G_{k} is the turbulence kinetic energy generated by the mean velocity gradients, G_{b} is the turbulence kinetic energy generated by buoyancy, and Y_{M} is the dilatation dissipation term. C_{μ}, σ_{ε}, σ_{k}, $C_{1\varepsilon}$, and $C_{2\varepsilon}$ are empirical constants with the following default values: C_{μ} = 0.09, σ_{ε} = 1.2, σ_{k} = 1, $C_{1\varepsilon}$ = 1.44, and $C_{2\varepsilon}$ = 1.92. S_{k} and S_{ε} are the user-defined source terms.

3.3.3. S2S Model

In radiant systems, radiative heat transfer accounts for a significant portion of total heat transfer. Therefore, the surface-to-surface (S2S) radiation model was used in the simulations. In this model, the radiation of a surface (k) is composed of both emission and reflection [31].

$$q_{\mathrm{k,out}} = \varepsilon_{\mathrm{k}} \sigma T_{\mathrm{k}}^4 + \rho_{\mathrm{k}} q_{\mathrm{k,in}} \tag{10}$$

where ε_{k} is the emissivity, σ is Boltzmann's constant, and $q_{\mathrm{k,in}}$ is the energy incident on the surface (k) from the surroundings, which is represented as a summation of radiation from the surrounding surface (j), as shown in Equation(11).

$$A_{\mathrm{k}} q_{\mathrm{k,in}} = \sum_{\mathrm{j}=1}^{\mathrm{N}} A_{\mathrm{j}} F_{\mathrm{jk}} q_{\mathrm{j,out}} \tag{11}$$

where A_k and A_j are the area of surface k and surface j (m^2), respectively; F_{jk} is the view factor between surface j and surface k; and $q_{j,out}$ is the radiative heat flux of the surface j (W/m^2).

3.3.4. Boussinesq Model

The Boussinesq model is used to model the natural convection in the closed space driven by buoyancy force. The model performs with the fluid density as a function of the temperature gradient as follows [31].

$$\left(\rho - \rho_0\right)g \approx -\rho_0\beta(T - T_0)g \tag{12}$$

where ρ_0 is the specified constant density of the flow, T_0 is the operating temperature, and β is the thermal expansion coefficient.

3.3.5. Other Equations

In addition, the total heat flux (q, W/m^2) is defined as the total heat transfer rate through all the panel surfaces divided by the panel surface area (A_s, m^2).

$$Q_{tot} = \frac{Q_{tot}}{A_s} \tag{13}$$

The radiation and convection heat transfer coefficient are then calculated based on the following equations.

$$H_r = \frac{Q_r}{A_s(AUST - T_p)} \tag{14}$$

$$h_c = \frac{Q_c}{A_s(T_a - T_p)} \tag{15}$$

where $AUST$ is the area-weighted uncooled temperature of the surfaces excluding the panel surface (°C), T_a is the air temperature (°C), and T_p is the panel surface temperature (°C).

Then, the operative temperature (T_{op}, °C) can be roughly determined by Equation (16).

$$T_{op} = \frac{h_c T_a + h_r \cdot AUST}{h_c + h_r} \tag{16}$$

3.4. Numerical Schemes

The governing equations are iteratively solved at each control volume in the computational domain until convergence is achieved. The Semi-Implicit Method for Pressure Linked Equations (SIMPLE) algorithm was applied for coupling pressure and momentum. The first-order upwind discretization scheme was chosen for turbulent kinetic energy and turbulent dissipation rate. The second-order upwind discretization scheme was used for the pressure, momentum, and energy. Enhanced wall treatment was selected as a wall treatment. The convergence criteria are 10^{-5} for all equations, with the exception of 10^{-6} for the energy equation.

3.5. Boundary Condition

Table 3 lists the boundary conditions and emissivity. The room is assumed to be well-insulated without heat transfer so that the envelope is assigned to the adiabatic condition. The non-uniform temperature distribution on the panel surface always occurs from the rise of chilled water or pipe arrangement. However, the temperature difference on the panel surface has less effect than the large difference between the air and the panel. Our study mainly focuses on optimizing the panel shape design based on heat transfer performance to improve the cooling capacity and indoor thermal condition. Therefore, the panel surface temperature is set constant at 15.83 °C, which is the experimentally measured value given

by Shin et al. [27]. Each panel design was investigated under seven different cooling load conditions (621.69 W, 746.03 W, 870.37 W, 994.71 W, 1119.04 W, 1243.38 W, and 1405.02 W), owing to differences in heat flux emitted from cylindrical dummies. In summary, 245 cases were simulated for analysis.

Table 3. Boundary condition and emissivity of each surface.

	Condition	Temperature (°C)	Heat Flux (W/m^2)	Emissivity
Wall/ceiling	adiabatic	-	0	0.82
Floor	adiabatic	-	0	0.95
Middle_plane	symmetry	-	-	-
Panel_surface	T = constant	15.83	-	0.92
Cylinder_outer	q = constant	-	50/60/70/80/90/100/113	0.92
Cylinder_upper	adiabatic	-	0	0.92

4. Results and Discussion

4.1. CFD Validation

The CFD model was validated with the experimental results for a flat panel presented by Shin et al. [27]. Figure 4 shows the air temperature distribution of the vertical measured line in three validation cases in which the cooling load was adjusted from 469.92 W to 1409.76 W. The simulated temperature showed marginal differences, with an average error of 1.01% in Case 1, 0.89% in Case 2, and 0.86% in Case 3, indicating that the CFD model agrees with the experimental measurements conducted for the freely suspended panel under different cooling load conditions.

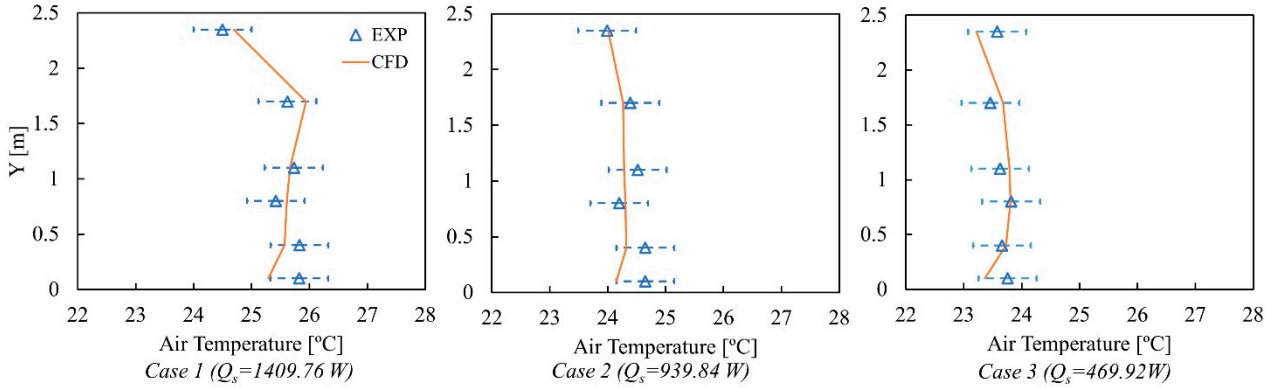

Figure 4. Comparison between CFD and experimental results reported by Shin et al. [27].

4.2. Panel Surface Temperature

Different ceiling radiant cooling panels can be compared and evaluated using the cooling capacity curve present in the standard [32], which is represented by the cooling capacity and the difference between the operative and panel surface temperature (Equation (17)). Previous studies [22,27] reported the curves under different cooling load conditions, adjusting the panel surface temperature to ensure that the indoor air temperature was within a comfort range. Nevertheless, in this study, the panel surface temperature was maintained at 15.83 °C in each case, with the cooling load increasing from 621.69 W to 1405.02 W.

Figure 5 compares the results of heat flux, heat transfer coefficient, average indoor air temperature, and the difference between operative and panel surface temperature, which were obtained under different panel surface temperature conditions. The panel surface temperature was set from 14.83 °C to 19.83 °C with an interval of 1 °C according to the design guidelines presented in [33]. Except for indoor air temperature increasing with the panel surface temperature increase, the heat flux and temperature difference were almost the same, with the difference maintained within 5%, indicating that different panel

surface temperature settings only affect indoor thermal conditions but not the panel cooling performance. The amount of heat transferred from the panel is related to the load and the panel itself rather than the surface temperature. Therefore, the boundary setting of this study was simplified.

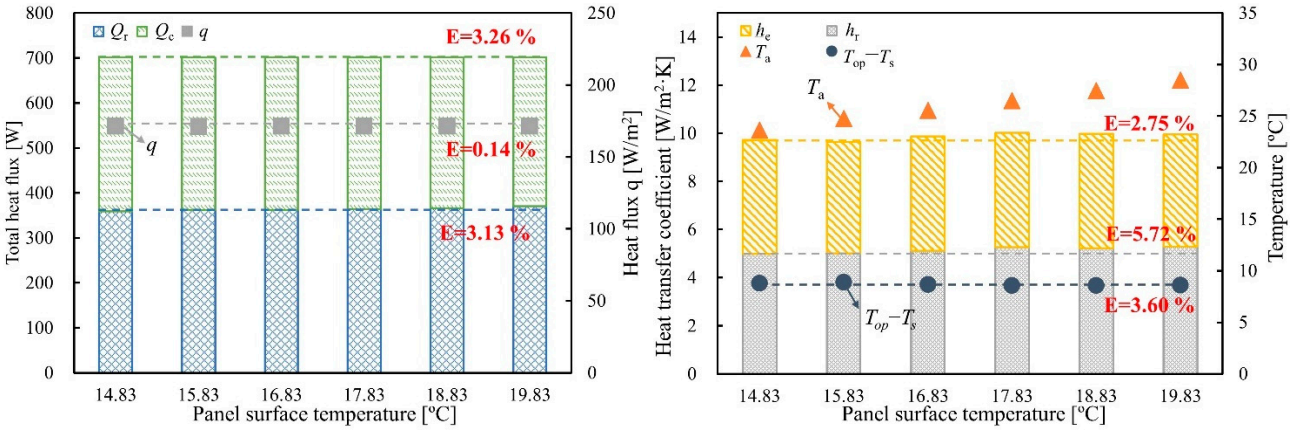

Figure 5. Calculation results under different panel surface temperatures.

4.3. Parametric Study

The cooling capacity of CRCPs is influenced by multiple factors—not only the panel design but also the cooling load, indoor condition, and panel surface temperature—making it difficult to evaluate and compare directly. Therefore, the cooling performance should be compared between different panel designs under a generalized operation condition. In this study, the cooling capacity was analyzed using power regression, which is in a functional relationship with the temperature difference between the operative and panel surface temperature as follows:

$$q = k(T_{op} - T_s)^n \quad (17)$$

The coefficient (k) and exponent (n) of each design are summarized in Appendix A. The nominal cooling capacity was obtained when the temperature difference was 8 K ($T_{op} - T_s$ = 8 K). All the designs were compared with a closed-type CRCP proposed in the European Standard [32], named 'Standard', and an open-type flat CRCP with a distributed layout proposed by Shin et al. [27], named 'A-d' in the following figures.

4.3.1. Panel Curvature Width

The effect of panel curvature width is shown by comparing the results of Design No.1–No.4. The curvature width (L) of Design 1, Design 2, Design 3, and Design 4 is 0.03 m, 0.06 m, 0.09 m, and 0.12 m, respectively. While the curvature radius is maintained at 0.06 m, and the void distance is maintained at 0.03 m. As shown in Figure 6, the cooling capacity and heat transfer coefficient decrease dramatically with increasing L. With a decrease in L from 0.12 m to 0.03 m, the nominal cooling capacity increases by 35.8% from 113.89 W/m^2 to 154.64 W/m^2. Additionally, both the h_r and h_c are improved significantly by 49.8% and 35%, respectively, under the same cooling load condition. Compared with Design 2 and Design 3, the convective heat transfer accounts for more in Design 1 and Design 4. Figure 7 compares the velocity contours in Design 1 and Design 4 under the highest cooling load. It is clear that the design with a shorter width contributes to accelerating the air moving through the openings around the panel to promote heat exchange.

4.3.2. Panel Curvature Radius

Figure 8 compares different curvature radii using the results from Design 5, Design 2, and Design No.6–No.9, with curvature radii 0.03 m, 0.06 m, 0.09 m, 0.15 m, 0.2 m, and 0.3 m, respectively. On the other hand, the panel curvature width is constant at 0.06 m, and the void distance is constant at 0.03 m. The results show that the cooling capacity

and heat transfer coefficient increase with increasing curvature radius. In particular, the nominal cooling capacity and radiation heat transfer coefficient are obviously improved by 9.1% and 36%, respectively, when r is increased from 0.03 m to 0.06 m. However, when r is larger than 0.06 m, the impact of increasing r is significantly reduced. The nominal cooling capacity and radiation heat transfer coefficient only increase by 4.2% and 3.9%, respectively, when r is increased from 0.06 m to 0.3 m.

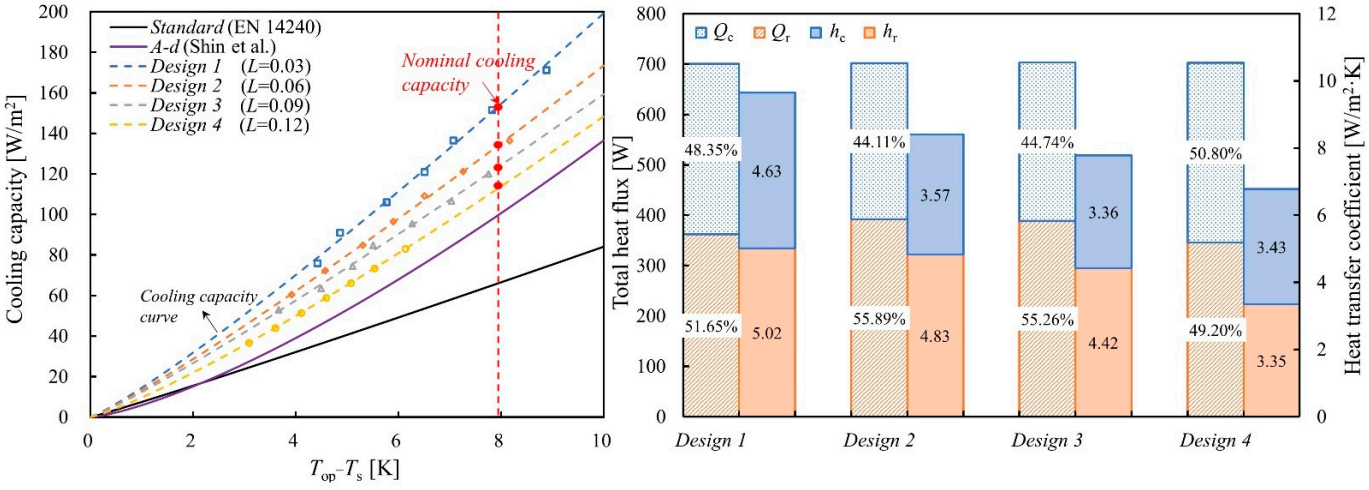

Figure 6. Comparison of different panel curvature lengths (**a**), cooling capacity curves [27,32] (**b**), and thermal performances under a cooling load of 1405.02 W.

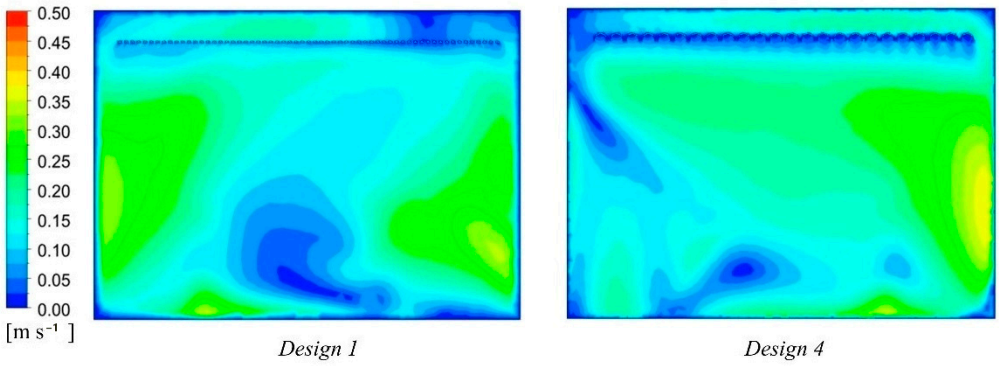

Figure 7. Velocity contours in Design 1 and Design 4 under a cooling load of 1405.02 W.

4.3.3. Void Distance

Figures 9 and 10 illustrate the effect of voids between adjacent panels or panel segments. Eight different distances were compared, varying from 0 m to 0.3 m, with L = 0.06 m and r = 0.06 m. A solid panel without an opening (Design 10) results in the same nominal cooling capacity as the CRCP proposed by Shin et al. When d is expanded from 0 m to 0.03 m, the nominal cooling capacity increases significantly by 33% from 101.27 W/m^2 to 134.69 W/m^2, and the h_r and h_c are improved by 6.4% and 92.9%, respectively. Including an opening between panels or panel segments can effectively increase convection heat transfer and enhance indoor air movement, as shown in the comparison of airflow distribution between Design 10 and Design 12 in Figure 10. The cooling capacity, h_r, and h_c continue to increase as the distance increases, but the growth slows when d is larger than 0.06 m. In particular, the nominal cooling capacity is highest in Design 16 when d is 0.21 m, which is 4.4% higher than that in Design 13, 13.3% higher than that in Design 12, and 50.1% higher than that in Design 10.

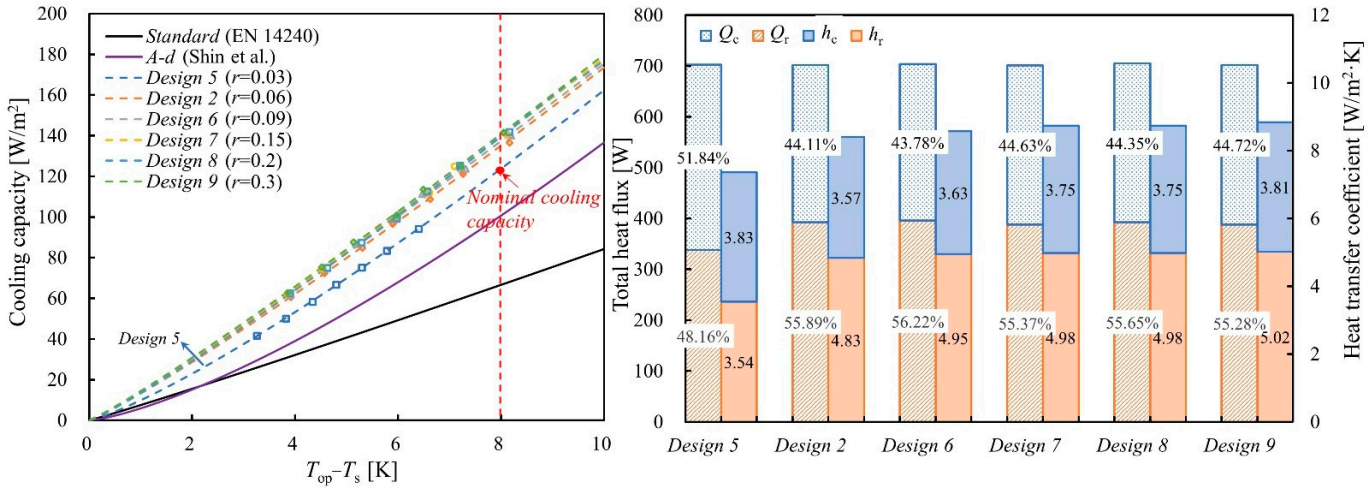

(**a**) (**b**)

Figure 8. Comparison of different curvature radii (**a**), cooling capacity curves [27,32] (**b**), and thermal performances under a cooling load of 1405.02 W.

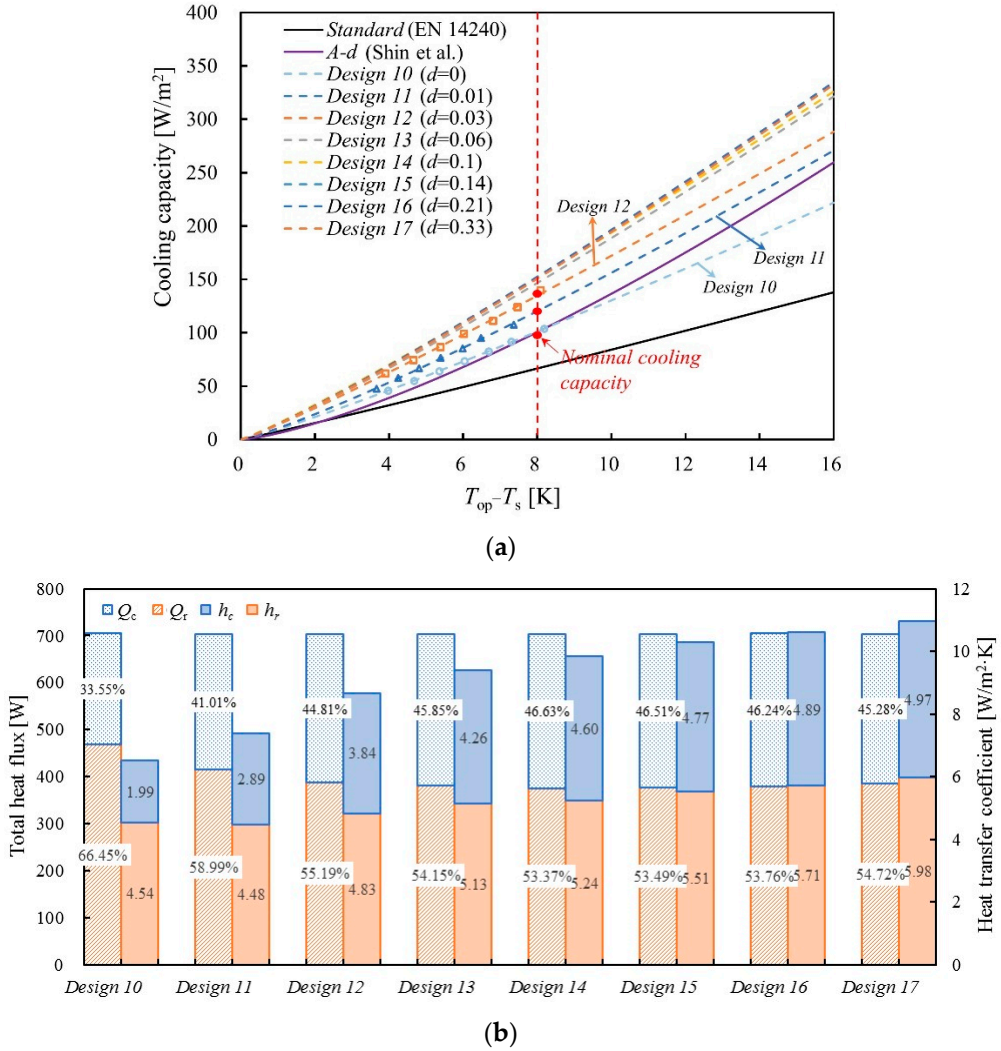

(**a**)

(**b**)

Figure 9. Comparison of different void distances (**a**), cooling capacity curves [27,32] (**b**), and thermal performances under a cooling load of 1405.02 W.

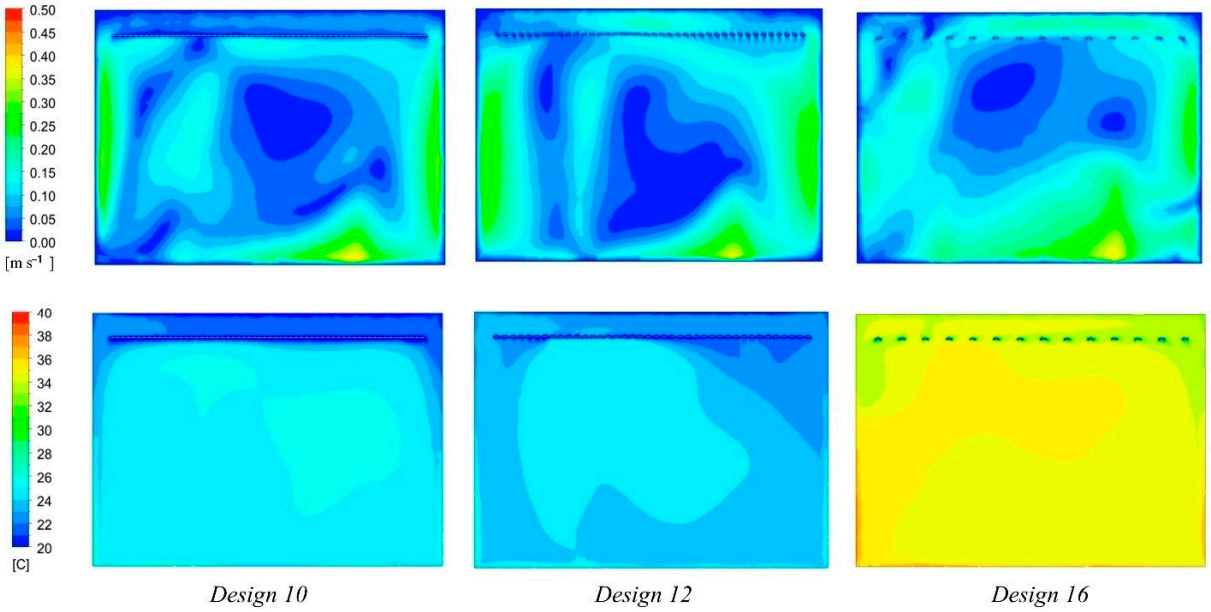

Figure 10. Velocity and temperature contours in Design 10, Design 12, and Design 16 under a cooling load of 1405.02 W.

The indoor air temperature in Design 16 is 10 °C higher than in Design 10 and Design 12, as shown in Figure 10, because the panel number in this design is too small to match the required total heat transfer amount. However, the air temperature uniformity in Design 16 is better than in the other two cases due to active air activity and sufficient heat exchange. The cooled air trapped on the top surface is allowed to move down, resulting in better cooling performance.

4.3.4. Coverage Area

The effect of coverage area was investigated by comparing Design 2 and Design No.18–No.22, as shown in Figure 11. When the coverage area is 11.43 m^2, the nominal cooling capacity is 12.8% higher than 7.58 m^2 and 5.8% higher than 12.96 m^2. The total heat transfer coefficient increases by 4.3% from 8.4 $W/m^2 \cdot K$ to 8.76 $W/m^2 \cdot K$ when the coverage area is reduced from 12.96 m^2 to 7.58 m^2. In other words, expanding the distance between the side of the panel and the wall within an appropriate range can enhance the cooling performance to the same extent as increasing the void distance between adjacent panels.

4.3.5. L/r Ratio and Surface Area

Two dependent parameters—L/r ratio and the panel surface area (A_s)—were examined with the other parameters unchanged. The L/r ratio is discussed by comparing Design No.23–No.27, as shown in Figure 12, which have the same void of 0.03 m and surface area of 11 $m^2 \pm 0.4$ m^2. As a result, when the L/r ratio is 0.5, the nominal cooling capacity is the highest, at 129.65 W/m^2, which is about 5% higher than that of the flat design. On the other hand, the h_c decreases by 12.2% and the h_r increases by 3.6% when the L/r is decreased from 1.1 to 0, illustrating that the curved shape can effectively promote air movement over the top surface and enhance convective heat transfer because the curved structure has a streamlined shape. Notably, when comparing the optimum design of $L/r = 0.5$ with the flat design, the h_c is increased by 5.3%, and h_r is maintained at the same value.

The panel surface area (A_s) was considered with an L/r ratio of 1.5 for the same void distance and panel coverage area, as shown in Figure 13. It should be noted that the L and r values are different in each design, as A_s is a dependent parameter related to all four independent design parameters. When A_s increases from 10.09 m^2 to 13.73 m^2, the nominal cooling capacity decreases by 15.2% from 136.11 W/m^2 to 118.20 W/m^2. The h_r and h_c in Design 28 are also 9.4% and 18.6% higher than those in Design 31, respectively. It is

concluded that the short and distributed panel design with less panel surface area achieves better cooling performance than the large solid panel design.

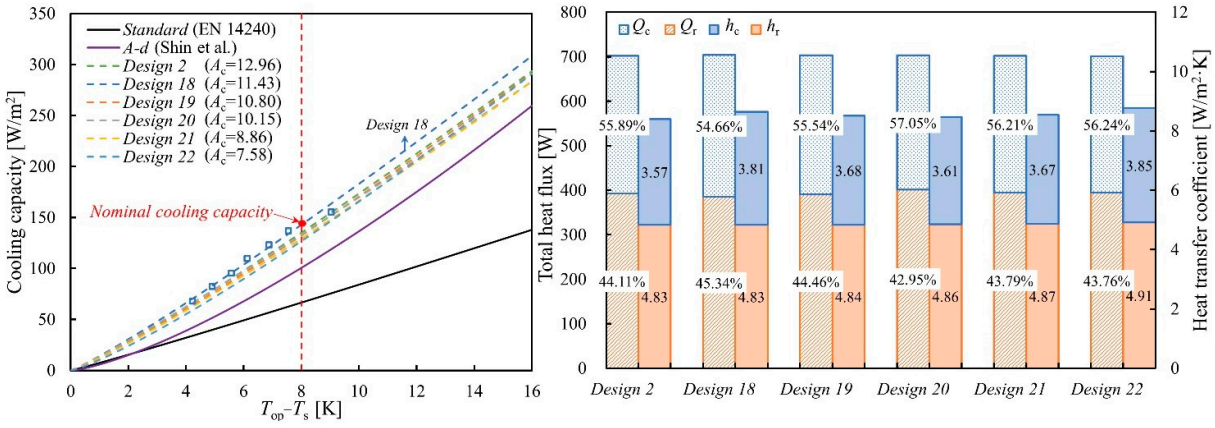

(**a**) (**b**)

Figure 11. Comparison of different coverage areas (**a**), cooling capacity curves [27,32] (**b**), and thermal performances under a cooling load of 1405.02 W.

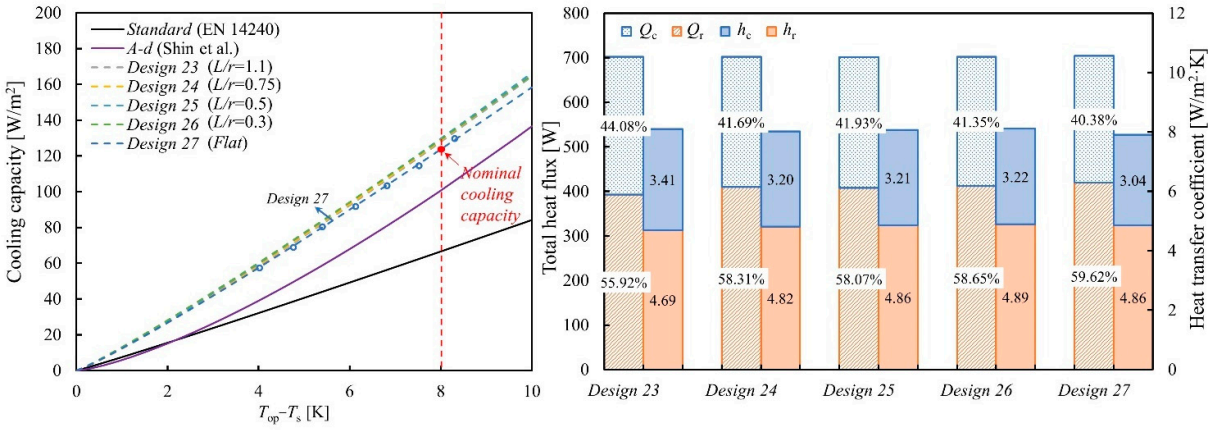

(**a**) (**b**)

Figure 12. Comparison of different L/r ratios (**a**), cooling capacity curves [27,32] (**b**), and thermal performances under a cooling load of 1405.02 W.

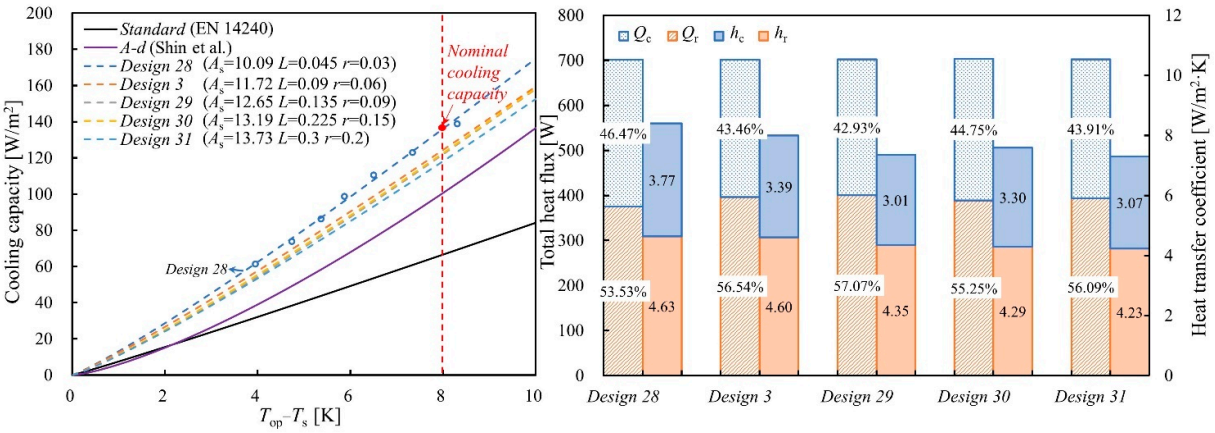

(**a**) (**b**)

Figure 13. Comparison of different surface areas (**a**), cooling capacity curves [27,32] (**b**), and thermal performances under a cooling load of 1405.02 W.

4.4. Sensitivity Measures

Based on the parametric analysis, the local sensitivity analysis of the effects of four independent design parameters on cooling capacity was carried out using the manual one-at-a-time (OAT) approach [34]. The sensitivities were measured by monitoring the changes in cooling capacity following the variation of one parameter while all other parameters were held constant. A linear regression equation was derived as a function of cooling capacity and each parameter. The results of sensitivity measures are summarized and compared in Figure 14. Consistent with the above conclusion, the void distance (d) plays the most crucial role in influencing cooling capacity, followed by panel curvature width (L) and radius (r). It is possible to achieve the same or even better indoor thermal conditions by applying fewer panels, demonstrating the potential for cost reduction by optimizing the panel arrangement and construction.

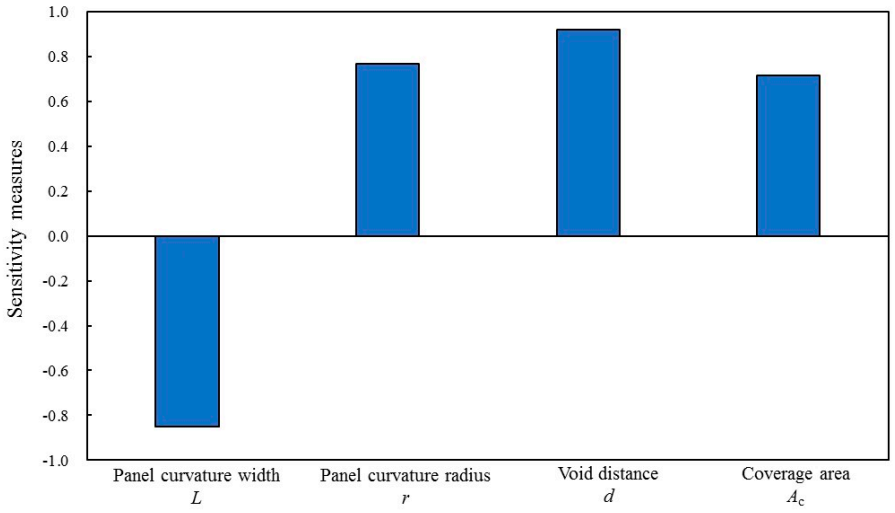

Figure 14. Sensitivity analysis of four dependent design parameters.

5. Discussion

Figure 15 shows the coefficient (k) and exponent (n) in Equation (17) of each panel design. It is clear that different panel designs achieve totally different cooling performances and that structural design is an effective way to improve the efficiency of the CRCP system. All the CRCP designs proposed in this study with curved and segmented shapes can achieve better cooling capacity than those proposed in previous studies under the same condition. Moreover, four designs (Design No.32–No.35) were replenished, combining the concluded optimum panel design of L = 0.03 m and r = 0.06 m with the void distance and coverage area. Figure 16 illustrates the flow and temperature fields on the symmetry plane in Design 1 and Design No.34–No.35. Design 34, with large openings between panels and between the panels and the wall, is the optimum among all the designs, if it prioritizes increasing the nominal cooling capacity. However, this design is unable to meet thermal comfort requirements under a cooling load of 1405.02 W in practice because of an insufficient number of panels. The temperature fields become more uniform in proposed Design No.34–No.35, but the average indoor temperature in Design 34 and Design 35 is about 4 K and 8 K higher than in Design 1, respectively. In regard to achieving both the thermal comfort conditions included in the ASHRAE standard [35] and maximum cooling capacity, Design 1 is the alternative optimum solution, which can maintain the indoor air temperature at 24.77 °C. Compared with Design 34, Design 1 has the same L and r values but with smaller opening areas. Therefore, (1) L = 0.03 m and r = 0.06 m represent the ideal panel shape, as concluded by comparing 35 designs in this study; (2) larger void distance and openings between panels and the wall are able to promote cooling capacity. However, preference should be given to thermal comfort and the number of required panels, which can be decided according to cooling capacity and panel surface area.

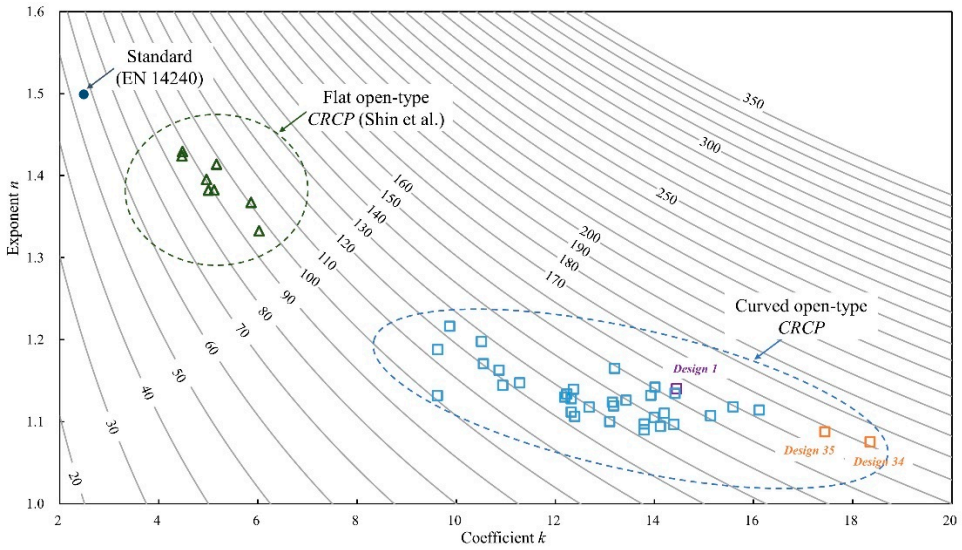

Figure 15. k and n of different CRCP designs ($T_{op} - T_s$ = 8 K) [27,32].

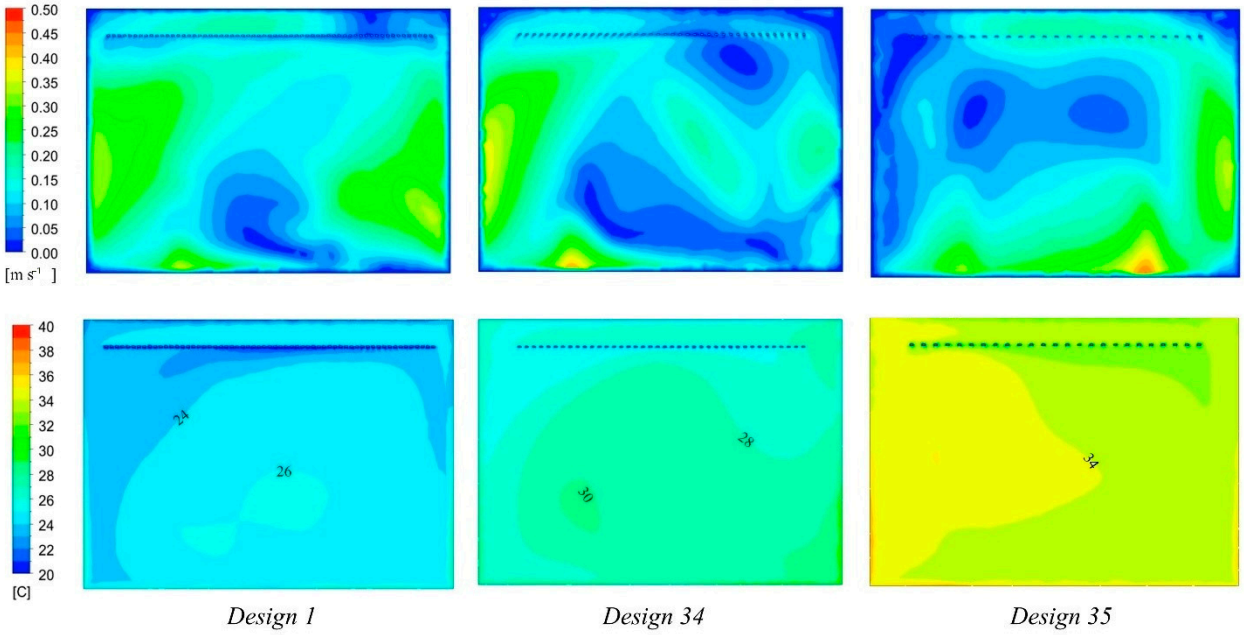

Figure 16. Velocity and temperature contours in Design 1, Design 34, and Design 35 under a cooling load of 1405.02 W.

Finally, we also recommend verifying the generalization of this optimum design by applying other models or experiments in future studies. Further improvements in CRCPs are also expected to be achieved through the application of advanced optimization methodology or the combination of different design strategies.

6. Conclusions

In this study, we carried out a parametric analysis of an open-type CRCP with a curved and segmented structure using CFD simulation to study the effect of panel structure on cooling capacity and heat transfer in comparison with conventional CRCPs presented in the literature. Four independent and two dependent design parameters were investigated by comparing thirty-five panel designs and operating sensitivity analysis. The optimal panel design was then proposed in terms of cooling capacity, heat transfer coefficient, and airflow distribution. The results are as follows:

- The freely suspended CRCP with curved shape and void in proposed this study achieves better cooling performance than the previous reference results. The nominal cooling capacity can be improved by 157.90% compared with the transitional panel design represented in the standard;
- The nominal cooling capacity and heat transfer coefficient increase with increasing panel curvature radius and decreasing curvature width. The nominal cooling capacity is highest when L = 0.03 m and r = 0.06 m, which is the optimal panel design among the designs proposed in this study;
- Compared with the large solid panel design, the short and distributed panel design with less panel surface area achieves better cooling performance because it can promote air movement around the panel and assist in sufficient heat exchange;
- The distances between adjacent panels and between the panel and the wall play the most significant role in improving the cooling performance of the panel, demonstrating the potential to simultaneously reduce costs and achieve better indoor thermal conditions by optimizing the distribution of CRCPs;
- There should be a balance between improving cooling performance and ensuring the comfort of the indoor environment in practical operations, and total heat transfer should be accounted for based on the panel surface area and cooling capacity.

Author Contributions: Conceptualization, A.A.S. and K.N.; methodology, M.Y.; validation, M.Y. and A.A.S.; formal analysis, M.Y.; investigation, M.Y.; writing—original draft preparation, A.A.S.; writing—review and editing, K.N.; supervision, K.N. All authors have read and agreed to the published version of the manuscript.

Funding: This work was supported by JSPS KAKENHI (grant number JP22J11117).

Data Availability Statement: The data presented in this study are available on request from the corresponding author.

Conflicts of Interest: The authors declare no conflict of interest.

Nomenclature

List of Symbols

L	Panel curvature width (m)
r	Panel curvature radius (m)
d	Void distance (m)
A_c	Panel coverage area (m^2)
A_s	Panel surface area (m^2)
l	Panel length (m)
n	Panel number (-)
ρ	Fluid density (kg/m^3)
$\vec{v}$	Velocity vector (m/s)
p	Static pressure (N/m^2)
$\vec{g}$	Gravitational body force (N/m^3)
$\vec{F}$	External body force (N/m^3)
μ	Molecular viscosity (kg/m·s)
I	Unit tensor
C_p	Specific heat capacity (J/kg·K)
T_f	Fluid temperature (K)
k_f	Fluid thermal conductivity (W/m·K)
k	Turbulent kinetic energy (m^2/s^2)
ε	Turbulent dissipation rate (m^2/s^3)
ε_k	Emissivity
σ	Boltzmann's constant
A_j, A_k	The area of surface j and k, respectively (m^2)
q_j, q_k	Radiative heat flux of surfaces j and k, respectively (W/m^2)
F_{jk}	View factor between surfaces j and k

ρ_0	Specific constant density of the flow (kg/m^3)
T_0	Operating temperature (°C)
β	Thermal expansion coefficient
q_{tot}	Total heat flux (W/m^2)
h_r	Radiation heat transfer coefficient (W/m^2·K)
h_c	Convection heat transfer coefficient (W/m^2·K)
$AUST$	Area-weighted uncooled temperature (°C)
T_p, T_s	Panel surface temperature (°C)
T_a	Air temperature (°C)
T_{op}	Operative temperature (°C)
Q_s	Cooling load (W)
CRCP	Ceiling radiant cooling panel
SRCP	Suspended radiant ceiling panel
CRP	Ceiling radiant panel
TCRP	Thermoelectric radiant panel
RCP	Radiant ceiling panel
CFD	Computational fluid dynamics

Appendix A

Table A1. Coefficient for nominal cooling capacity equation.

	k	n	R^2	$q_{\Delta T = 8K}$ (W/m^2)
Standard [33]	7.489	1.051	-	66.6
A-d [26]	5.8604	1.3674	-	100.6
Design 1	14.448	1.14	0.9949	154.64
Design 2	13.178	1.1193	0.9983	135.11
Design 3	12.321	1.1118	0.9957	124.37
Design 4	9.626	1.1882	1	113.89
Design 5	9.8661	1.2165	0.9997	123.81
Design 6	14.118	1.0942	0.9976	137.38
Design 7	13.994	1.1053	0.9974	139.36
Design 8	13.427	1.1261	0.9991	139.62
Design 9	14.392	1.0968	0.9986	140.81
Design 10	9.6204	1.132	0.9999	101.27
Design 11	10.549	1.1707	0.9984	120.35
Design 12	13.795	1.0974	0.9965	134.69
Design 13	13.927	1.1322	0.9994	146.67
Design 14	15.133	1.1075	0.9981	151.39
Design 15	13.196	1.165	0.9997	148.78
Design 16	14.418	1.1346	0.9994	152.60
Design 17	14.01	1.1421	0.9992	150.61
Design 18	14.198	1.1104	0.9843	142.90
Design 19	12.365	1.1398	0.9987	132.29
Design 20	13.795	1.0901	0.9987	133.10
Design 21	12.23	1.1338	0.9996	129.23
Design 22	10.507	1.1978	0.9978	126.82
Design 23	12.19	1.13	0.9989	127.79
Design 24	12.321	1.128	0.9979	128.63
Design 25	12.68	1.118	0.9951	129.65
Design 26	13.098	1.1004	0.9983	129.11
Design 27	12.39	1.1065	0.9989	123.69
Design 28	13.149	1.1239	0.9943	136.11
Design 29	10.864	1.1631	0.9901	122.00
Design 30	11.279	1.1475	0.9941	122.62
Design 31	10.94	1.1445	0.9998	118.20
Design 32	15.585	1.1182	0.9985	159.42
Design 33	16.117	1.1143	0.9996	163.53
Design 34	18.354	1.0754	0.9932	171.76
Design 35	17.442	1.0877	0.9997	167.45

References

1. Rhee, K.N.; Kim, K.W. A 50 Year Review of Basic and Applied Research in Radiant Heating and Cooling Systems for the Built Environment. *Build. Environ.* **2015**, *91*, 166–190. [CrossRef]
2. Imanari, T.; Omori, T.; Bogaki, K. Thermal Comfort and Energy Consumption of the Radiant Ceiling Panel System. *Energy Build.* **1999**, *30*, 167–175. [CrossRef]
3. Dudkiewicz, E.; Jadwiszczak, P.; Jeżowiecki, J. Examination of Operational Dynamics of Radiant Ceiling Panel. *Cent. Eur. J. Eng.* **2011**, *1*, 159–167. [CrossRef]
4. Miriel, J.; Serres, L.; Trombe, A. Radiant Ceiling Panel Heating-Cooling Systems: Experimental and Simulated Study of the Performances, Thermal Comfort and Energy Consumptions. *Appl. Therm. Eng.* **2002**, *22*, 1861–1873. [CrossRef]
5. Ye, M.; NAGANO, K.; Serageldin, A.A.; Sato, H. Field Study on Energy Consumption and Thermal Comfort of a Nzeb Using Radiant Ceiling Panel and Open-Loop Groundwater Heat Pump System in a Cold Region. *J. Build. Eng.* **2023**, *67*, 105999. [CrossRef]
6. Memon, R.A.; Chirarattananon, S.; Vangtook, P. Thermal Comfort Assessment and Application of Radiant Cooling: A Case Study. *Build. Environ.* **2008**, *43*, 1185–1196. [CrossRef]
7. Valdiserri, P.; Cesari, S.; Coccagna, M.; Romio, P.; Mazzacane, S. Experimental Data and Simulations of Performance and Thermal Comfort in a Patient Room Equipped with Radiant Ceiling Panels. *Buildings* **2020**, *10*, 235. [CrossRef]
8. Tye-Gingras, M.; Gosselin, L. Comfort and Energy Consumption of Hydronic Heating Radiant Ceilings and Walls Based on CFD Analysis. *Build. Environ.* **2012**, *54*, 1–13. [CrossRef]
9. Feng, J.; Bauman, F.; Schiavon, S. Experimental Comparison of Zone Cooling Load between Radiant and Air Systems. *Energy Build.* **2014**, *84*, 152–159. [CrossRef]
10. Park, S.H.; Kim, D.W.; Joe, G.S.; Ryu, S.R.; Yeo, M.S.; Kim, K.W. Establishing Boundary Conditions Considering Influence Factors of the Room Equipped with a Ceiling Radiant Cooling Panel. *Energies* **2020**, *13*, 1684. [CrossRef]
11. Xing, D.; Li, N. Thermal Performance Improvement for the Ceiling Radiant Cooling Panel with an Inbuilt Air Gap by the Convection Shield. *Sustain. Energy Technol. Assessments* **2021**, *44*, 101012. [CrossRef]
12. Labat, M.; Lorente, S.; Mosa, M. Influence of the Arrangement of Multiple Radiant Ceiling Panels on the Radiant Temperature Field. *Int. J. Therm. Sci.* **2020**, *149*, 106184. [CrossRef]
13. Zhang, L.; Liu, X.H.; Jiang, Y. Experimental Evaluation of a Suspended Metal Ceiling Radiant Panel with Inclined Fins. *Energy Build.* **2013**, *62*, 522–529. [CrossRef]
14. Jordan, S.; Hafner, J.; Kuhn, T.E.; Legat, A.; Zbašnik-Senegačnik, M. Indoor Environment in Retrofitted Offices Equipped with Radiant Ceiling Panels. *Gradjevinar* **2016**, *68*, 125–134. [CrossRef]
15. Xing, D.; Li, N.; Zhang, C.; Heiselberg, P. A Critical Review of Passive Condensation Prevention for Radiant Cooling. *Build. Environ.* **2021**, *205*, 108230. [CrossRef]
16. Shakya, P.; Ng, G.; Zhou, X.; Wong, Y.W.; Dubey, S.; Qian, S. Thermal Comfort and Energy Analysis of a Hybrid Cooling System by Coupling Natural Ventilation with Radiant and Indirect Evaporative Cooling. *Energies* **2021**, *14*, 7825. [CrossRef]
17. Jeong, J.W.; Mumma, S.A. Ceiling Radiant Cooling Panel Capacity Enhanced by Mixed Convection in Mechanically Ventilated Spaces. *Appl. Therm. Eng.* **2003**, *23*, 2293–2306. [CrossRef]
18. Shin, M.S.; Choi, J.S.; Rhee, K.N. Cooling Capacity and Energy Performance of Open-Type Ceiling Radiant Cooling Panel System with Air Circulators. *Energies* **2021**, *14*, 5. [CrossRef]
19. Ye, M.; Serageldin, A.A.; Radwan, A.; Sato, H.; Nagano, K. Thermal Performance of Ceiling Radiant Cooling Panel with a Segmented and Concave Surface: Laboratory Analysis. *Appl. Therm. Eng.* **2021**, *196*, 117280. [CrossRef]
20. Lim, H.; Kang, Y.K.; Jeong, J.W. Thermoelectric Radiant Cooling Panel Design: Numerical Simulation and Experimental Validation. *Appl. Therm. Eng.* **2018**, *144*, 248–261. [CrossRef]
21. Luo, Y.; Zhang, L.; Liu, Z.; Wang, Y.; Wu, J.; Wang, X. Dynamic Heat Transfer Modeling and Parametric Study of Thermoelectric Radiant Cooling and Heating Panel System. *Energy Convers. Manag.* **2016**, *124*, 504–516. [CrossRef]
22. Serageldin, A.A.; Ye, M.; Radwan, A.; Sato, H.; Nagano, K. Numerical Investigation of the Thermal Performance of a Radiant Ceiling Cooling Panel with Segmented Concave Surfaces. *J. Build. Eng.* **2021**, *42*, 102450. [CrossRef]
23. Mosa, M.; Labat, M.; Lorente, S. Constructal Design of Flow Channels for Radiant Cooling Panels. *Int. J. Therm. Sci.* **2019**, *145*, 106052. [CrossRef]
24. Mosa, M.; Labat, M.; Lorente, S. Role of Flow Architectures on the Design of Radiant Cooling Panels, a Constructal Approach. *Appl. Therm. Eng.* **2019**, *150*, 1345–1352. [CrossRef]
25. Hassan, M.A.; Kaood, A. Multi-Criteria Assessment of Enhanced Radiant Ceiling Panels Using Internal Longitudinal Fins. *Build. Environ.* **2022**, *224*, 109554. [CrossRef]
26. Radzai, M.H.M.; Yaw, C.T.; Lim, C.W.; Koh, S.P.; Ahmad, N.A. Numerical Analysis on the Performance of a Radiant Cooling Panel with Serpentine-Based Design. *Energies* **2021**, *14*, 4744. [CrossRef]
27. Shin, M.S.; Rhee, K.N.; Park, S.H.; Yeo, M.S.; Kim, K.W. Enhancement of Cooling Capacity through Open-Type Installation of Cooling Radiant Ceiling Panel Systems. *Build. Environ.* **2019**, *148*, 417–432. [CrossRef]
28. Radwan, A.; Katsura, T.; Ding, L.; Serageldin, A.A.; EL-Seesy, A.I.; Nagano, K. Design and Thermal Analysis of a New Multi-Segmented Mini Channel Based Radiant Ceiling Cooling Panel. *J. Build. Eng.* **2021**, *40*, 102330. [CrossRef]

29. Lv, G.; Shen, C.; Han, Z.; Liao, W.; Chen, D. Experimental Investigation on the Cooling Performance of a Novel Grooved Radiant Panel Filled with Heat Transfer Liquid. *Sustain. Cities Soc.* **2019**, *50*, 101638. [CrossRef]
30. Ning, B.; Chen, Y.; Liu, H.; Zhang, S. Cooling Capacity Improvement for a Radiant Ceiling Panel with Uniform Surface Temperature Distribution. *Build. Environ.* **2016**, *102*, 64–72. [CrossRef]
31. ANSYS FLUENT 12.0/12.1 Documentation. Available online: https://www.afs.enea.it/project/neptunius/docs/fluent/index.htm (accessed on 31 January 2023).
32. *EN 14240*; Ventilation for Buildings-Chilled Ceilings-Testing and Rating. CEN: Brussels, Belgium, 2004.
33. *ISO 11855-2:2012(E)*; Building Environment Design-Design, Dimensioning, Installation and Control of Embedded Radiant Heating and Cooling Systems. Part 2: Determination of the Design Heating and Cooling Capacity. International Organization for Standard: Geneva, Switzerland, 2012.
34. Borgonovo, E.; Plischke, E. Sensitivity Analysis: A Review of Recent Advances. *Eur. J. Oper. Res.* **2016**, *248*, 869–887. [CrossRef]
35. *ANSI/ASHRAE 55-2013*; ASHRAE Standard: Thermal Environmental Conditions for Human Occupancy. American Society of Heating, Refrigerating and Air-conditioning Engineers Inc.: Atlanta, GA, USA, 2013.